Microporous and Mesoporous Materials 181 (2013) 208–216

Contents lists available at ScienceDirect

Microporous and Mesoporous Materials

journal homepage: www.elsevier.com/locate/micromeso

From rays to structures: Representation and selection of void structures in zeolites using stochastic methods

Andrew J. Jones [a], Christopher Ostrouchov [b,c], Maciej Haranczyk [c], Enrique Iglesia [a,d,*]

[a] Department of Chemical and Biomolecular Engineering, University of California, Berkeley, CA 94720, United States
[b] Department of Applied Mathematics, Clemson University, Clemson, SC 29631, United States
[c] Computational Research Division, Lawrence Berkeley National Laboratory, Berkeley, CA 94720, United States
[d] Chemical Sciences Division, Lawrence Berkeley National Laboratory, Berkeley, CA 94720, United States

ARTICLE INFO

Article history:
Received 25 March 2013
Received in revised form 19 July 2013
Accepted 27 July 2013
Available online 2 August 2013

Keywords:
Zeolite
Void
Pore
Monte Carlo
Ray

ABSTRACT

Voids within crystalline microporous solids are represented here using stochastic distributions of rays placed and oriented randomly within the accessible void space, represented using Voronoi decompositions. This algorithm is provided in the Zeo++ software for open use. In this method, ray lengths are depicted as two-dimensional histograms that complement alternate descriptors, such as free and included sphere diameters. We illustrate the specific use of these methods as a tool to narrow the range of zeolites useful for a given catalytic application because of the shape and size of voids. DAC, AFS, AFY, SFO and EON zeolites contain void spaces similar, as suggested by Euclidean distance values between histograms, to those within MOR 8-MR side pockets, which stabilize the transition states that mediate dimethyl ether carbonylation to methyl acetate; these alternate structures offer different connecting void environments, which can enhance or restrict molecular access and influence the effectiveness of the 8-MR protons. NES, EON and USI zeolites exhibit histogram features similar to those of 12-MR MOR channels, where protons selectively catalyze alkylation of biphenyl and naphthalene to 4,4′-diisopropylbiphenyl and 2,6-diisopropylnaphthalene, respectively, with propene. SBT, FAU and SBS contain voids similar in topology to the 12-MR channels of LTL zeolites, within which Pt clusters remain active and stable during the dehydrocyclization of light alkanes, but without the one-dimensional nature of LTL channels. The approach and implementation of these methods are applicable to any microporous or mesoporous solids and to adsorption processes driven by van der Waals contacts between hosts and guest molecules.

1. Introduction

Zeolites have crystalline microporous frameworks with ordered channels, windows and cages 0.3–1.9 nm [1] in size. As catalytic materials, their narrow pore size distributions exclude molecules larger than their connecting channels and windows [2] and their small voids preferentially solvate certain transition states and reactants, giving rise to specific reactivity and shape selectivity [3–7]. Emerging protocols for the synthesis of solids with diverse pore topologies [1,8] continue to increase the diversity of available frameworks, currently more than 190 [9], which represent, however, only a small fraction of the >500,000 thermodynamically feasible structures [10]. Such a breadth of distinct frameworks requires algorithms to describe and visualize their void spaces, so as to choose a specific zeolite structure for a given application in adsorption and catalysis [11].

The largest included sphere (D_i) and free sphere (d_f) diameters [12], determined using Delaunay triangulation of zeolite frameworks, provide single-valued descriptors of three-dimensional zeolite pores; they are currently provided in the web-based International Zeolite Association Database (IZA) [9]. These diameters define the largest spheres that can be contained in (D_i) or diffuse through a given structure (d_f). More recently, the deconstruction of accessible pores into a collection of geometric shapes, such as spheres and cylinders [13], has proven useful for inspecting pore environments; they yield a breadth of information, such as poreconnectivities, volumes and surface areas. The corrugations and non-spherical void shapes, which may be important for solvation of non-spherical molecules, are not accurately represented by these methods. Hologram representations of zeolite voids based on Voronoi decompositions [14] provide another descriptor of zeolite voids, but it is unclear how the Voronoi node edge length, a measure of size, relates to the size scales relevant for the van der

* Corresponding author at: Department of Chemical Engineering, University of California, 201 Gilman Hall, Berkeley, CA 94720, United States. Fax: +1 510 642 4778.
E-mail address: iglesia@berkeley.edu (E. Iglesia).

1387-1811/$ - see front matter © 2013 Elsevier Inc. All rights reserved.
http://dx.doi.org/10.1016/j.micromeso.2013.07.033

Waals interactions that matter for catalysis and adsorption processes. Methods that rely on the characterization or classification of frameworks [15,16] focus on elementary building blocks of zeolites instead of the void spaces that they form and which carry significant consequences for adsorption and catalysis. More robust descriptors for the characterization and selection of zeolites as adsorbents and catalysts must includeinformation about the void shape, size, corrugation and connectivity in a simpler and more interpretable and retrievable format.

Here, we present a new method to describe size and shape of voids and their non-uniform distributions in microporous solids. The emphasis is on zeolites and related inorganic solids, but the approach is generally applicable to porous solids. The algorithm determines the distribution of ray lengths in accessible void spaces resulting in a void space fingerprint that describes pore topologies in two-dimensions; it is similar but complementary to pore size distributions [17] and contains retrievable information about the surface texture, shape and size of void spaces. These ray-trace histograms are useful in visualizing and selecting microporous structures for specific catalytic and adsorption applications. Ray-trace calculations are implemented in the Zeo++ open-source suite [18,19]. We show here how histograms can be used to find zeolite structures with overall void spaces similar in shape, size and corrugation to those in MFI zeolites from IZA and hypothetical zeolite databases using Euclidean distance metrics. The results of such a similarity search are used to examine the consequences of void environment on light alkane dehydrocyclization on Pt clusters in LTL, carbonylation of dimethyl ether by eight-member (8-MR) MOR pockets, and alkylation of naphthalene and biphenyl in 12-MR MOR channels, and in doing so to identify candidates with similar void spaces but different connectivity within the IZA zeolite structure database.

2. Methods

2.1. Computation of ray lengths in zeolite voids

The ray trace algorithm utilizes Voronoi decomposition protocols implemented in Zeo++ [18,19] to provide the required void accessibility details based on spherical probes and framework atoms of user-specified size. The Voronoi decomposition is an efficient method to access detailed information about the void space geometry and topology, especially when compared with alternate grid-based approaches [20,21]. In this study, the coordinates of framework atoms for 194 zeolite structures contained in the IZA database [9] and 139, 396 hypothetical thermodynamically feasible zeolite structures (within +30 kJ mol^{-1} of Si α-quartz) [10] that are accessible to a free sphere of diameter 0.325 nm (e.g. CH_4) are used together with the van der Waals radii for O and Si atoms (0.152 and 0.210 nm, respectively, reported for zeolites [22]) to construct ray histograms for each microporous structure. Zeolite structures are imported into the Zeo++ program in crystallographic information file (CIF) formats. We refer to all structures as zeolites in this work, although some are not currently available in their aluminosilicate form.

The Monte Carlo algorithm reported here places a point at a random position within a zeolite unit cell. Accessible volumes (V_a) and surface areas (SA_a) are determined as those that can be reached by the center of a spherical probe of diameter 0.1 nm. We consider such a probe to be large enough to exclude environments inaccessible to common molecules used as reactants, but small enough to accurately represent the relevant channel corrugations and texture. We examine two implementations that we denote as *constrained* and *unconstrained*. In the *constrained* approach, only ray origins that happen to be contained within V_a of the void structure are considered and rays are grown in a random direction until they intersect with the surface of a pore. This process is repeated in the opposite direction to define a ray that intersects the surface of a void at two points. Periodic boundary conditions are implemented with a defined cutoff length of 10 nm in order to terminate the infrequent rays that traverse through voids without encountering two intersections over 10 nm. In the *unconstrained* ray trace method, the starting point and direction of a ray within a unit cell are selected randomly without reference to the accessible volume. The intersection points of this ray with the surface of each pore that it crosses within a distance of 10 nm are recorded and are used to determine the lengths of rays contained within the entire internal volume. In both implementations, the length and number of rays are recorded and grouped in 1000 bins, each 0.01 nm wide, to create ray-trace histograms. Unless specified otherwise, histograms were created with 1,000,000 sample points for IZA zeolites and 100,000 sample points for hypothetical zeolites. The algorithm has been implemented within Zeo++ and is available online [19].

2.2. Algorithm for determining similarity among histograms

Similarities among ray histograms were determined using a Euclidean distance formula. This metric was selected because of its simplicity in logic and execution and of its sensitivity to the shape of histogram features, which contain details about the shape of the voids they represent, thus permitting pore topologies for different structures to be compared in detail. There are several other approaches to determine similarity and their comparison for various purposes is addressed elsewhere [17] and is beyond the scope of this study.

The Euclidean distance formula calculates the sum of the square of the differences between the probability density of rays of two samples in each bin i, for all bins:

$$S_{d,euc} = \sqrt{\sum_{i=1}^{n}(P_{1,i} - P_{2,i})^2} \quad (1)$$

here, $S_{d,euc}$ is the Euclidean distance defined for the two samples being compared (1 and 2), where $P_{j,i}$ is the probability density of rays in bin i for sample j, normalized so that the sum of the probability densities multiplied by the bin size, x, is unity:

$$1 = \sum_{i=1}^{n} P_{j,i} \cdot x \quad (2)$$

3. Results and discussion

3.1. Stochastic ray projections and their frequency in MFI

Fig. 1 shows the density, location, and lengths of randomly placed and oriented rays in a MFI zeolite supercell using the *constrained* approach, in which ray origins are selected at random from the portion of the void structure accessible by a 0.1 nm sphere. Rays fill the sinusoidal and straight 10-MR channels of MFI, as well as the ellipsoidal voids created at their intersections, resulting in different ranges of ray lengths and distributions for each specific region within the void space. Higher densities of rays are present within larger pore volumes, because they have higher probabilities of containing ray origins and projections. Short rays (0–0.3 nm, Fig. 1a) lie near the surface of the voids, where intersections of rays with the same pore surface are more frequent. The corrugations present in sinusoidal channels result in a higher density of short rays in their voids relative to straight channels. Rays with lengths between 0.3 and 0.6 nm (Fig. 1b) intersect channels

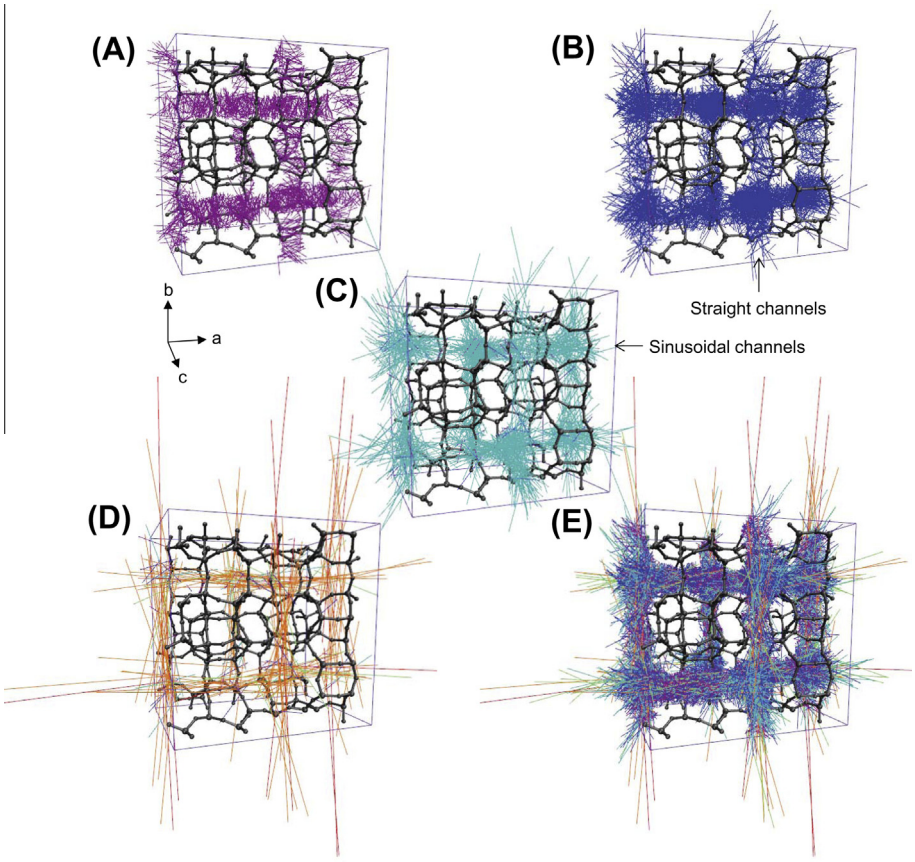

Fig. 1. Illustration of randomly placed and oriented rays using the *constrained* method in MFI with framework Si and O atoms added for clarity. Rays are displayed according to their length: (a) 0–0.3 nm, (b) 0.3–0.6 nm, (c) 0.6–0.9 nm, (d) larger than 1.2 nm, and (e) 0–10 nm.

almost perpendicular to their direction and occur most frequently (Fig. 2). Rays of 0.6–0.9 nm length (Fig. 1c) are predominantly located within the voids formed by intersections of straight and sinusoidal channels. Rays longer than 1.2 nm (Fig. 1d) traverse beyond channel intersections, but occur rarely (Fig. 2). Thus, the collection of all rays describes the size of void environments because longer rays are present in larger volumes.

The ensemble of ray lengths can be converted into a histogram (Fig. 2) to depict the unique pore topology of each zeolite in two-dimensions. In Fig. 2, the frequencies of rays in MFI voids are shown as a function of their length such that the total area under the histogram is unity. In the case of MFI, rays with 0.40 nm length are most abundant, as shown by its prominent feature in the histogram. This feature is the result of a large number of rays that cross pores along their diameter (Fig. 1b). We can compare this value to the channel diameters in MFI reported in the IZA database by increasing ray lengths by 0.134 nm to account for the differences between the van der Waals radii of the O-atoms (0.135 nm [12]) and the probe diameter used to determine accessible surface areas. The feature at 0.40 nm (adjusted to 0.53 nm) is consistent with the diameter of channels (0.51–0.56 nm; [9]); it appears at ray lengths slightly larger than the diameter of the largest sphere that can freely traverse MFI (0.446–0.470 nm; [9]). The breadth of this feature is affected by the shape of the pore, with more elliptical pores exhibiting somewhat more bimodal features (e.g., see MOR in Section 3.3) with the two radii of the ellipse given by the peak positions in the histogram. The shape is also affected by the presence of sinusoidal channels in MFI, which lead to a higher frequency of smaller rays and thus to another feature at shorter ray lengths.

The other feature in the ray-trace histogram of MFI (at 0.82 nm, Fig. 2) arises from voids at channel intersections (Fig. 1c). Weaker

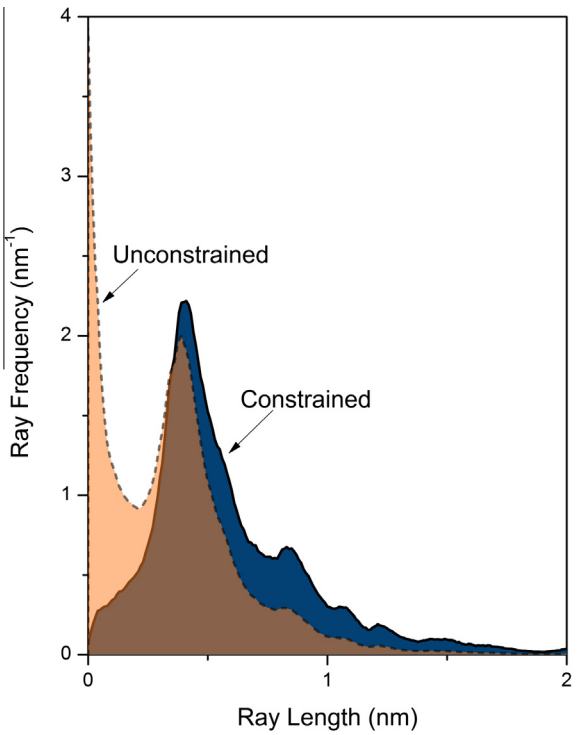

Fig. 2. Ray trace histograms normalized so the area under each curve is unity for MFI with 6.1 million rays placed randomly within the void structure using the *unconstrained* approach normalized (dotted line) and 2.1 million rays with the *constrained* approach (solid line).

features are observed in the histogram for ray lengths beyond 0.82 nm and correspond to rays that extend beyond one unit cell (Fig. 1d). Rays that extend beyond one unit cell traverse straight and sinusoidal channels with increasingly high probabilities of intersecting void surfaces reflected by the small area of these features in ray histograms.

The number, location and shape of peaks in a ray histogram are specific to each zeolite structure and correspond to specific void environments, such as channels and intersections in the case of MFI. While ray histograms provide an easy method to represent, interpret and retrieve pore landscapes, the transformation of a three-dimensional ensemble of rays into a two-dimensional histogram results in a loss of information about the connectivity and asymmetry of voids. In addition, distinct void environments, when similar in size, can result in overlapping features in a ray histogram, such as the features from sinusoidal and straight channels in MFI. A natural extension of ray histograms would be to separate histograms for each distinct pore environment. For example, the ray histogram of MFI could be divided into contributions from rays contained within straight channels, sinusoidal channels and channel intersections. Yet, most zeolites contain a small number of unique void environments, which are either significantly different in size and would create unique histogram features or are similar enough in size that they would behave similarly in catalytic and adsorption processes.

Fig. 2 compares the probability densities of rays found in MFI using the *unconstrained* and *constrained* methods. Both methods lead to histograms with peaks at 0.40 nm and 0.82 nm and thus represent channels and intersections with similar histogram features. The *unconstrained* method, however, has a larger fraction of rays shorter than 0.14 nm. These rays are predominantly located near the surfaces of voids and become less prominent in the *constrained* approach because ray origins that lie near the edges of accessible void spaces occupy a smaller fraction of the void space and are therefore selected less frequently during sampling. Rays shorter than 0.14 nm do not describe features that are consequential for adsorption or catalysis because molecules of interest are typically larger than such volumes. This suggests that the *constrained* method is more appropriate for comparisons among samples and it is the method that we use in the rest of this study.

The average void environment for all zeolites in the IZA database [9] and the Hypothetical Zeolite Database [10] can be represented by the sum of the probability densities of rays for each zeolite. Fig. 3a shows the results of this summation using the *constrained* method for MFI and for all zeolites in the two databases. The features in the IZA composite histogram contain three main differences from the MFI histogram: (1) a bimodal feature clustered ~0.1 nm around the MFI channel diameters (0.28–0.50 nm), (2) no distinguishable features above 0.40 nm, and (3) a slight feature at 0.06 nm. These differences suggest that IZA zeolites contain voids that are similar in size to MFI but with a bimodal distribution most likely corresponding to 8-MR and 10-MR channels. This is consistent with the scarcity of single structures larger than 0.8 nm and a nearly bimodal distribution of largest free sphere diameters [13]. Figs. 3b and 3c show the position of the largest feature in ray histograms compared with the diameter of the largest included and free spheres calculated using similar parameters with the Zeo++ program for zeolites in the IZA and hypothetical databases, respectively. A large fraction of zeolite frameworks have a similar feature position and sphere diameter, as indicated by their proximity to the parity line, implying that ray histogram peak positions are similar to sphere diameters as concluded previously for MFI. Sphere diameters and ray peaks cluster in two distinct regions around 0.40 nm for IZA zeolites (Fig. 3b) consistent with the composite histogram in Fig. 3a and the interpretation that 8-MR and 10-MR channels dominate voids in IZA zeolites. Zeolites far

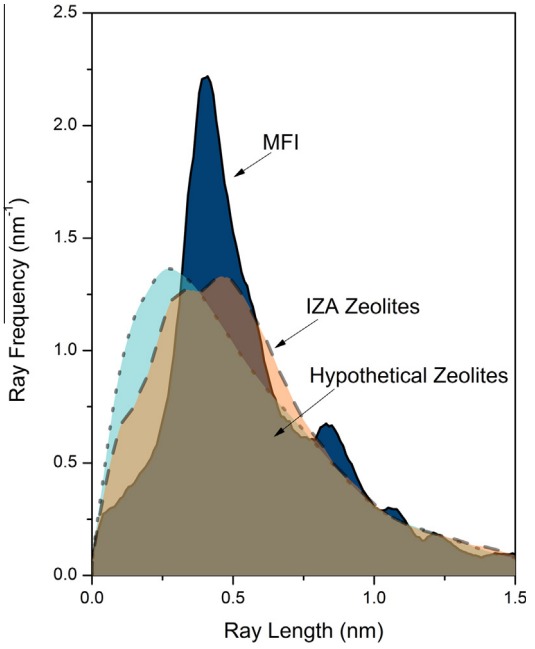

Fig. 3a. Ray trace histogram of MFI (blue; solid line) and the average of ray frequencies for IZA zeolites (orange; dashed line) and hypothetical zeolites accessible to a spherical probe of 0.325 nm diameter (green; dotted line) using the *constrained* approach. (For interpretation of the references to color in this figure legend, the reader is referred to the web version of this article.)

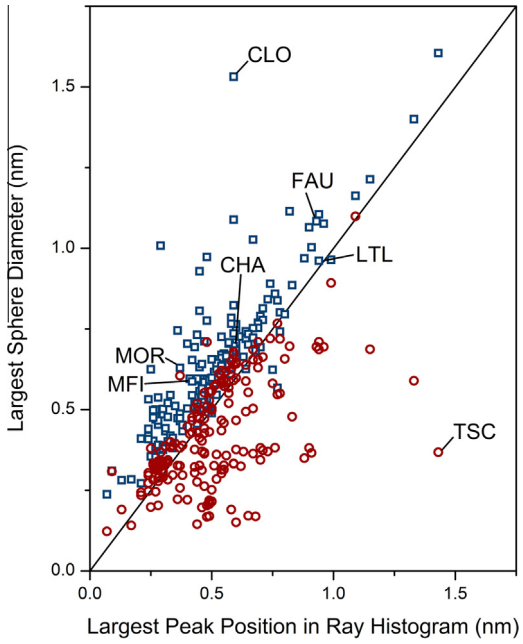

Fig. 3b. Comparison of largest free (red circle) and included (blue square) sphere diameters with the position of the largest feature in ray trace histograms for zeolites in the IZA database using the *constrained* approach calculated with Zeo++ using equivalent probe and van der Waals parameters. Outliers and some common zeolites are identified. Solid parity line is drawn to guide the eye. (For interpretation of the references to color in this figure legend, the reader is referred to the web version of this article.)

from the parity line (Fig. 3b) result when the largest sphere diameter is not representative of the void space with the largest fraction of void volume, because the largest histogram feature contains, by definition, the largest frequency of rays, which are selected at random from the void space and thus occur more frequently in larger volumes.

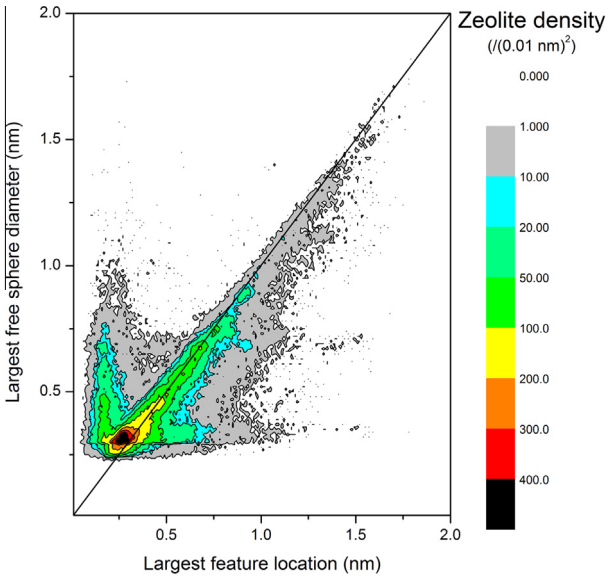

Fig. 3c. Density contour plot comparing zeolite descriptors for ~140,000 zeolites in the Hypothetical Zeolite Database. Largest free sphere diameters and the largest feature in ray trace histograms are calculated using the *constrained* approach with Zeo++ using equivalent probe and van der Waals parameters. Solid parity line is drawn to guide the eye.

The ray-average void size of zeolites contained in the Hypothetical Zeolite Database is 0.14 nm smaller than the channels in MFI (Fig. 3a), even though these zeolites were screened for accessibility to a CH_4 probe. This is also apparent from the large density of hypothetical zeolites with largest features around 0.26 nm in Fig. 3c. Smaller pores occur concurrently with larger atom densities in the unit cells (higher framework densities), which are thermodynamically more stable, consistent with the abundance of structures with ~0.26 nm size in stable zeolites. The small number of outliers from the parity line in Fig. 3c suggests that for the majority of hypothetical zeolites, voids with the largest volume fraction (represented by the largest feature in ray histograms) represent the same voids as those probed with the largest free sphere diameter; this is probably due to a high prevalence of channels because cage-window structures would lead to smaller free sphere diameters than largest ray histogram features.

3.2. Finding zeolites with similar structural features as MFI

The previous section illustrates how ray histograms describe pore environments and resolve void features important for adsorption and catalysis. Next, we show how ray histograms can be compared to identify zeolites with pore and void characteristics similar to one another. As an example, structures in the IZA database [9] are compared with MFI by computing the Euclidean distance between their individual histograms and that for MFI. The Euclidean distance value allows relative similarity comparisons for various structures with a given (query) structure (e.g. TER and STW each with respect to MFI) but its magnitude is arbitrary unless appropriately normalized by the difference between the maximum and minimum Euclidean distances amongst all zeolites in a search set. This normalization, however, is not required for the determination of similar voids, which is the focus of this study; the comparison of absolute similarity is discussed in detail in another study [17].

Table 1 lists the Euclidean distance for the most and least similar zeolites to MFI, when all features smaller than 5.0 nm are included in ray histograms, along with largest sphere diameters, dimensionalities and largest ring sizes. TER (intersecting straight and sinusoidal 10-MR channels with cage-like intersections), STW (tortuous 10-MR channels with cage-like voids on the side of channels) and SVR (intersecting tortuous 10-MR channels) zeolites emerge as void structures most similar to MFI. The histograms and void structures of these three zeolites and MFI are shown in Figs. 4 and 5, respectively. The structures all have 10-MR channels, but their similarity is not readily apparent from a visual inspection of their voids, as represented in Fig. 5, because the voids do not have the same straight and sinusoidal channels and intersections present in MFI. A recent study showed that the isosteric heats of adsorption of CO_2 are similar for Na^+-MFI and Na^+-SVR zeolites [23] suggesting that their pore environments may indeed be similar for this specific practical purpose, consistent with their similar ray histograms.

The histogram for TER (Fig. 4) resembles that for MFI both visually and in its Euclidean distance ($S_{d,euc} = 0.129$), which is the smallest among IZA zeolites. Features at 0.81 and 1.17 nm are present in both MFI and TER histograms (Fig. 4), suggesting that the distances between larger voids (those represented by a peak at 0.81 nm) are similar in these two structures; indeed the distances between channel intersections in both MFI and TER are separated by ~1.0 nm.

STW and SVR do not contain intersecting straight and sinusoidal channels, while MFI and TER do; yet, all four samples give similar histograms, suggesting that their voids are similar in shape and size. STW and SVR contain tortuous channels and cage-like voids of similar size to the channel intersections in MFI, based on the ray histograms. This is not evident by visual inspection of the tortuous channels in STW and SVR (Fig. 5) or from their included or free sphere diameters (Table 1), which would predict that channels and intersection sizes differ by as much as 0.1 nm between STW and MFI (largest included sphere diameters of 0.543 and 0.636 nm, respectively). Included and free sphere diameters are not suitable for this comparison because spherical models do not accurately represent the shape of channels and intersections in STW and SVR. In contrast, details of any arbitrary shape are present within the ray-trace histogram features, for example the ellipsoidal channel intersections in MFI show a broad feature at 0.81 nm and the ellipsoidal side-pockets in MOR show a bimodal feature (see Section 3.3.1).

The similar void sizes and shapes of MFI, TER, STW and SVR voids and channels suggest that reactants and transition states will be stabilized similarly by van der Waals interactions in these voids, which can have large consequences on catalytic reactivity [5]; but, their different pore connectivities, orientations and tortuosities would have significant consequences for diffusional access. Thus, the similarity of structures from ray histogram metrics can narrow the selection of potential candidate structures for catalytic or adsorption evaluation.

Next, we examine the differences between ray histograms and the range of Euclidean distances between MFI and other structures.

Table 1
Summary of structures most (dis)similar to MFI determined from ray histograms.

Structure	$S_{d,euc}$[a]	D_i (nm)[b]	d_f (nm)[b]	Dimensionality	Largest ring size
MFI	0.000	0.636	0.470	3	10
TER	0.129	0.694	0.516	2	10
STW	0.135	0.543	0.488	3	10
SVR	0.137	0.585	0.465	3	10
BCT	0.377	0.380	0.291	1	8
LIT	0.411	0.324	0.181	0	8
VSV	0.439	0.294	0.197	3	9
Average[c]	0.243	0.680	0.451	N/A	N/A

[a] Euclidean distance from MFI determined for rays between 0 and 5 nm.
[b] Maximum included (D_i) and free sphere diameters (d_f) [9].
[c] Average values from zeolite structures in IZA database [12].

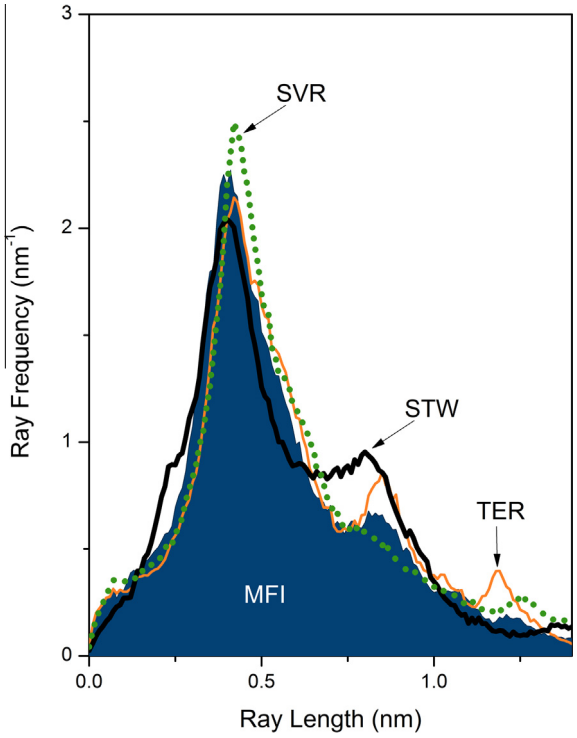

Fig. 4. Ray histograms of MFI (solid blue) and IZA zeolites with minimum Euclidean distances from MFI calculated for rays with lengths between 0 and 5 nm: TER (thin orange line), STW (thick black line), and SVR (green dotted line). (For interpretation of the references to color in this figure legend, the reader is referred to the web version of this article.)

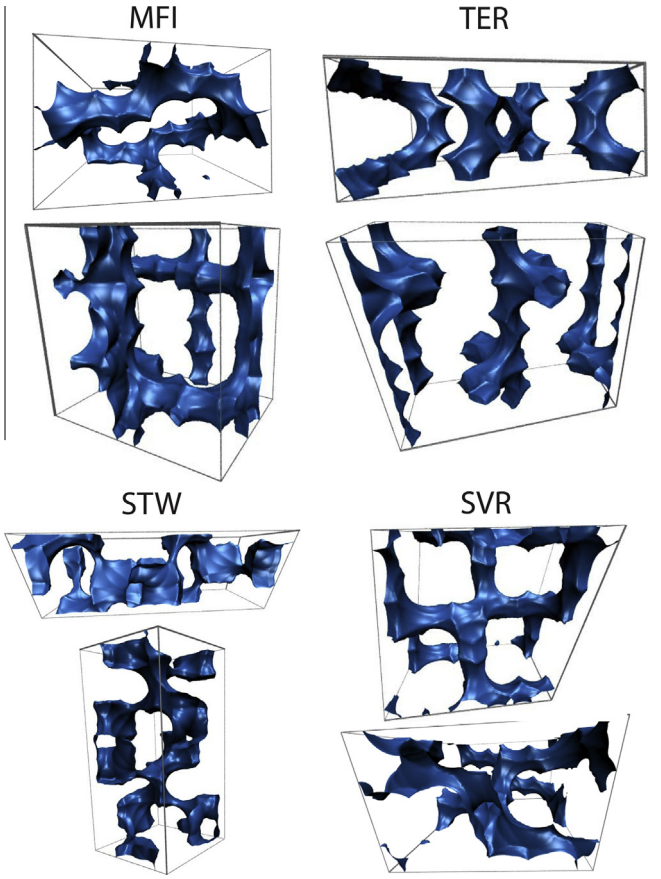

Fig. 5. Pore landscapes for MFI, TER, STW and SVR zeolites determined from the surface area accessible to the center of a spherical probe with a 0.1 nm diameter and O and Si van der Waals radii of 0.152 nm and 0.210 nm, respectively.

Euclidean distance values of MFI with respect to IZA zeolites extend from 0.129 to 0.439 (see Supporting information) and differ in magnitude for each zeolite, except for BEC and ISV, which give a Euclidean distance of 0.262. A similarity test between BEC and ISV shows that the histograms are indeed similar ($S_{d,euc}$ = 0.098), but not identical, which would result in a distance value of zero. We infer that histograms for each zeolite in the IZA database contain a unique distribution of features and thus histograms provide a fingerprint of the void environment of each zeolite. The least similar zeolites to MFI include BCT, LIT and VSV with Euclidean distance values of 0.377, 0.411 and 0.439, respectively. These samples contain small 8-MR channel structures that are very different from 10-MR channels in shape and size, consistent with their large Euclidean distances.

The abbreviated results of a similarity search between MFI and ~140,000 hypothetical zeolites are included in the Supporting information. The frameworks identified in the search are inaccessible to current synthetic protocols, however, they demonstrate how zeolite framework selection could be accomplished with ray histograms when synthetic hurdles are overcome.

3.3. The use of ray-trace histograms and similarity metrics to select void structures for specific purposes

This section demonstrates, using three illustrative examples, how ray histograms can be used to find candidate catalytic solids that can stabilize specific transition states with high selectivity via similarity searches. The concept that voids and channels can solvate reactants and transition states through van der Waals interactions and that, in doing so, can influence reactivity or selectivity is widely accepted and exploited in the practice of zeolite catalysis [1,24]. For example, n-pentane cracking turnover rates vary over a range of 10^3 with pore size for zeolites with pores that vary by 0.2 nm [5]. Many studies have reported the ubiquitous stabilization of transition states and reactants via van der Waals stabilization [2,25–29].

3.3.1. Selective carbonylation of dimethyl ether to methyl acetate

The carbonylation of dimethyl ether (DME) to methyl acetate occurs selectively at bound methyl groups located within 8-MR side pockets in MOR or 8-MR channels of FER; turnover rates are not detectable at sites within 10-MR or 12-MR channels or in cages or channel intersections of MFI, BEA or FAU [30]. Theoretical treatments have recently suggested that the shape of 8-MR side pockets in MOR and the relative orientation of the methyl are responsible for the increase in selectivity to carbonylation [31]. Alternate and possibly better carbonylation catalysts would contain 8-MR pockets or channels similar in size and shape to 8-MR side pockets in MOR, but connected via multi-dimensional larger channels to allow molecular flow. The shape and size of 8-MR side pockets in MOR are represented by a histogram feature between 0.12 and 0.46 nm in Fig. 6, which can be used in a ray histogram similarity search to find other zeolites with similar voids. A selection of zeolite frameworks determined from a similarity search for ray histograms with features similar to those in MOR in the region between 0.12 and 0.46 nm are summarized in the top portion of Table 2 with their ray histograms compared in Fig. 6. DAC (10-MR straight channels with 8-MR void windows that connect these channels) emerges as the IZA zeolite with the most similar side pockets to those in MOR, but its 10-MR connecting channels are smaller than channels in MOR and may impose diffusional

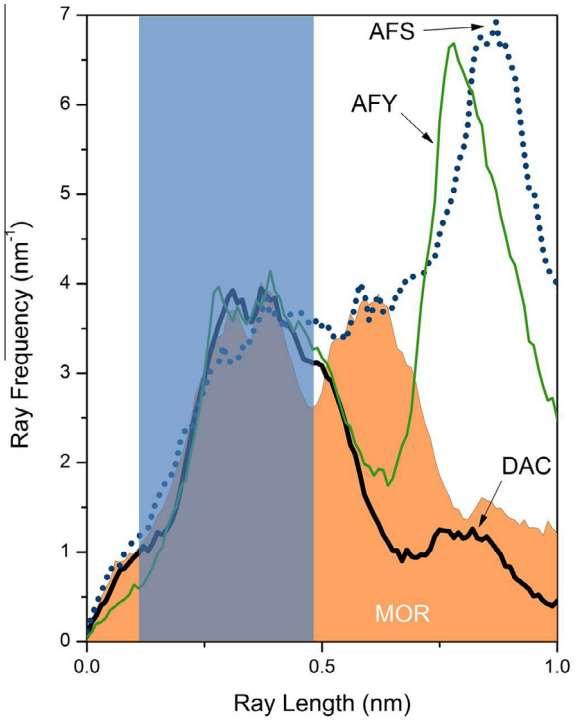

Fig. 6. Ray histograms of MOR (solid orange) and IZA zeolites with minimum Euclidean distances from MOR calculated for rays with lengths between 0.12 and 0.46 nm (area highlighted by blue box), which are contained mostly in the 8-MR side pockets in MOR: DAC (thick black line), AFS (blue dotted line), and AFY (thin green line). Ray histograms are normalized to compare the feature at 0.12–0.46 nm by dividing ray frequencies by the total number of rays in this range for each zeolite. (For interpretation of the references to color in this figure legend, the reader is referred to the web version of this article.)

Table 2
Summary of structures similar to 8-MR side pockets (DAC, AFS, AFY, SFO and EON) and 12-MR channels (NES, EON and USI) in MOR determined from ray histograms with ray lengths between 0.12–0.46 nm and 0.47–2.0 nm, respectively.

Structure	$S_{d,euc}$[a]	D_i (nm)[b]	d_f (nm)[b]	Dimensionality	Largest ring size
MOR	0.000	1.001	0.750	1	12
DAC	0.118	0.528	0.419	2	10
AFS	0.141	0.951	0.601	3	12
AFY	0.148	0.782	0.590	3	12
SFO	0.156	0.792	0.695	2	12
EON	0.157	0.783	0.679	2	12
NES	0.124	0.704	0.507	2	10
EON	0.139	0.783	0.679	2	12
USI	0.145	0.676	0.628	2	12
Average[c]	0.236	0.680	0.452	N/A	N/A

[a] Euclidean distance from MOR.
[b] Maximum included (D_i) and free sphere diameters (d_f) [9].
[c] Average values from zeolite structures in IZA database from [12] for 8-MR side pocket similarity.

constraints. These possible transport restrictions can be avoided by probing the most similar zeolites to choose those with free sphere diameters larger than 0.55 nm [12]; the four resulting zeolites within the ten most similar are AFS, AFY, SFO and EON (Table 2). The shape and size of the 8-MR voids in these samples should cause any H^+ (and the CH_3 groups that replace them) to exhibit the transition state stabilization that confers high DME carbonylation reactivity to 8-MR side pockets in MOR. We note that AFS, AFY and SFO are not currently available as aluminosilicates and therefore H^+, when present in their voids, may differ in acid strength and reactivity from H^+ species in MOR. The EON structure (Table 2) is of particular interest because its 8-MR channels connect parallel 12-MR channels, in contrast with the dead-end nature of the MOR side pockets; this feature may allow faster diffusion within the micropore structure. As this example indicates, these similarity metrics based on ray histograms can focus the synthesis and catalytic evaluation efforts on the most promising structures in both IZA and hypothetical databases of zeolites and also allow the testing of competing hypotheses to account for the reactivity of specific structures.

3.3.2. Isopropylation of biphenyl and naphthalene by large-pore zeolites

Next, we search for zeolites with voids similar to the 12-MR channels of MOR, which are selective for isopropylation of biphenyl and naphthalene to 4,4′-diisopropylbiphenyl and 2,6-diisopropylnaphthalene, respectively [32–34]. Rays between 0.47 and 2.0 nm in ray histograms are contained within 12-MR channels of MOR; thus, a similarity search using this histogram feature may identify zeolites with similar void shape and size to these channels. Table 2 shows the resulting three zeolite frameworks from this similarity search (NES, EON, USI) and compares their Euclidean distances from 12-MR MOR, as well as their largest sphere diameters, dimensionalities, and largest ring sizes.

NES (intersecting 10-MR straight and sinusoidal channels) shows the smallest Euclidean distance ($S_{d,euc} = 0.124$) from 12-MR MOR channels, in spite of the exclusive presence of 10-MR windows; this reflects the sinusoidal shape of these NES channels, which create local voids larger than expected from its 10-MR structure. In this case, the window size and largest sphere descriptors would have led to an incorrect conclusion of dissimilarity with MOR channels (e.g., the largest included sphere diameters of MOR and NES are 1.0 and 0.70 nm, respectively). EON emerges as a zeolite with similar 12-MR channels as MOR and, as discussed in Section 3.3.1, also contains voids similar to the side pockets in MOR. The similarity of shape and size of both void environments in EON and MOR make EON a particularly interesting case also for comparisons of DME carbonylation reactivity.

We consider last USI zeolites (intersecting 10-MR and 12-MR channels) with 12-MR channels similar in shape and size to MFI, but also containing intersecting 10-MR channels that create a void that is slightly larger than in 12-MR MOR channels and which are likely to increase the rate of formation of the less desirable di-isopropyl bulkier isomers [32]. This illustrates how similarity searches based on ray histograms can identify similar voids but often require further interrogation when the connectivity of voids becomes important. These examples demonstrate that ray histograms often lead to frameworks that are non-obviously similar from largest sphere diameter metrics (Table 2). Similarity searches with ray histograms can greatly reduce the analysis time and increase the accuracy of structure comparisons compared with searches based on sphere diameter descriptors or visual inspections of frameworks. In this case, the method is able to identify a handful of structures as promising candidates for the selective isopropylation of biphenyl and naphthalene to their least bulky products.

3.3.3. Determining the mechanism for stabilization of Pt in LTL

Next, we examine how ray histograms can be used to discriminate among structures based on long range void shapes, such as the undulating channel constrictions present in LTL. Pt clusters within LTL (one-dimensional 12-MR channels) zeolites have been used for dehydrocyclization of C_6–C_9 alkanes to form arenes [35–39]; the unique reactivity of these clusters has been ascribed to inhibition of oligomerization reactions, which lead to unreactive carbon residues, by the one-dimensional nature of LTL channels [35,40,41]. It is unclear whether the one-dimensional nature or the size and shape of the channels are responsible for the

protection of the encapsulated Pt clusters. Structures with channels of similar size and shape but interconnected in two or three dimensions would allow us to discern the relative contributions of connectivity and local structure to inhibited deactivation.

We have calculated Euclidean distance statistics between ray histograms for LTL and other frameworks in the IZA database for rays 0.5–1.2 nm long, which represent the portion of the histograms describing the channel structure of LTL. SBT (intersecting 12-MR channels with large cages), FAU (large cages connected by 12-MR windows), and SBS (intersection 12-MR sinusoidal and straight channels with large cages) are identified as structures with voids most similar to the undulating channels in LTL (Table 3). Fig. 7 displays the ray histograms for LTL, SBT, FAU and SBS, and demonstrates the similarity in feature shape and position between these zeolites. The pore systems in SBT, FAU and SBS also constrict and open to cage-like voids with included sphere diameters of 1.00–1.15 nm, but with three-dimensional networks absent in LTL. This void three-dimensionality can shed light on the structural basis for the stabilization of Pt clusters within LTL channels. Dealuminated FAU zeolites have been shown to mitigate deactivation of confined Pt clusters more than clusters of equivalent size on mesoporous SiO_2, but not to the same extent as LTL [40]. These results support the hypothesis that the connectivity differences between FAU and LTL are responsible for their stability differences, because local "containers" for Pt clusters are similar in the two samples based on their similar ray histograms.

A search for structures similar to LTL based on the closest free or included sphere diameters identifies structures (ETR, UFI, LTN, MAZ, AFI, and AET) with a wide variety of largest pore openings (8–18 MR) and void networks with entirely straight channels or cages connected by 8-MR windows (Table 3). Structures with 8-MR windows (UFI and LTN) are impractical because such windows prevent access and egress of reactants and products. Structures with larger windows (ETR, MAZ, AFI, and AET) lack the shape of pores found in LTL which may be important for the stabilization of Pt and could explain why Pt contained in 12-MR channels of MOR are not stable [42]. Thus, included and free sphere diameters are useful for describing pore size for spherical cages or straight channels but they neglect the shape that many zeolite voids exhibit, which ray histograms capture and which are likely to be consequential for catalysis.

The identification of zeolites with voids similar to the 10-MR channels and intersections in MFI, the 8-MR side pockets and 12-MR channels in MOR, and the 12-MR channels in LTL demonstrate the ability of ray histograms to distinguish and select void environments with catalytic consequences because of their shape and size, but with potentially different void connections. Euclidean distance metrics provide a straightforward method for the comparison of histogram features and therefore, the voids that they represent, providing a narrow selection of zeolites with potential catalytic applications. These tools complement existing void descriptors, such as inscribed and free sphere diameters, by describing void shape instead of just size and allow for the evaluation of specific void features from large databases of structures.

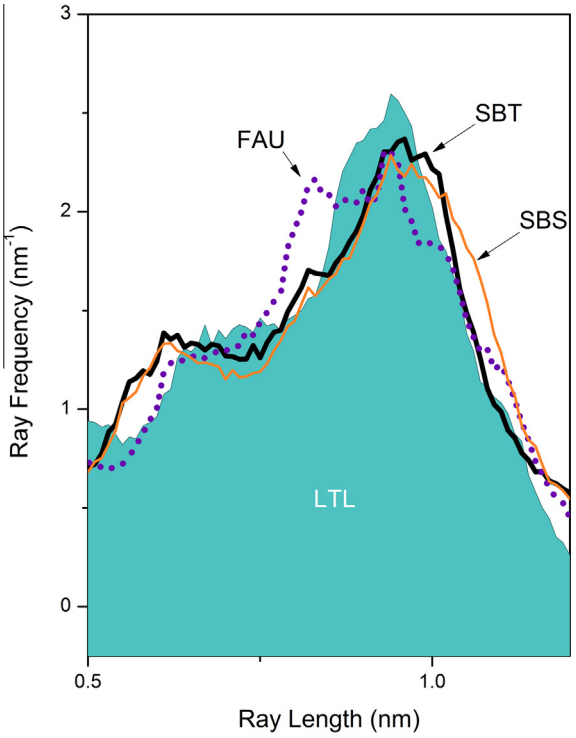

Fig. 7. Ray histograms of LTL (solid blue) and IZA zeolites with minimum Euclidean distances from LTL calculated for rays with lengths between 0.5 and 1.2 nm, which are contained in the 12-MR channels of LTL: SBT (thick black line), FAU (purple dotted line), and SBS (thin orange line). Ray histograms are normalized to compare the feature at 0.5–1.2 nm by dividing ray frequencies by the total number of rays in this range for each zeolite. (For interpretation of the references to color in this figure legend, the reader is referred to the web version of this article.)

Table 3
Summary of structures similar to LTL determined from ray histograms between 0.5 and 1.2 nm (SBT, FAU and SBS) and largest included sphere diameters (ETR, UFI and LTN).

Structure	$S_{d,euc}$[a]	D_i (nm)[b]	d_f (nm)[b]	Dimensionality	Largest ring size
LTL	0.000	1.001	0.750	1	12
SBT	0.129	1.117	0.734	3	12
FAU	0.139	1.124	0.735	3	12
SBS	0.147	1.145	0.727	3	12
ETR	0.206	1.005	0.933	3	18
UFI	0.209	1.009	0.389	2	8
LTN	0.315	1.013	0.208	0	8
Average[c]	0.329	0.680	0.452	N/A	N/A

[a] Euclidean distance from LTL.
[b] Maximum included (D_i) and free sphere diameters (d_f) [9].
[c] Average values from zeolite structures in IZA database from [12] for 8-MR side pocket similarity.

4. Conclusions

A method is presented for the characterization and comparison of zeolite voids through the Monte Carlo sampling of rays in accessible volumes of microporous structures. Ensembles of rays are represented by two-dimensional ray histograms, which encode the details of pore shapes, sizes and distributions in complex void networks. Ray histograms complement previous descriptors of void space such as largest free and included sphere diameters, largest ring openings and accessible surface areas and volumes, by describing void shape instead of just size and by describing the distribution of void environments within a zeolite. We demonstrate with illustrative examples how ray histograms describe the unique pore environments of MFI, MOR and LTL, and utilize the features present in their histograms to find structures in IZA and hypothetical zeolites databases with similar catalytically relevant voids using a simple Euclidean distance similarity metric. The algorithm determines void similarities amongst large databases of nearly 140,000 hypothetical and existing zeolite frameworks on the order of minutes with specificity to void sizes and shapes which matter for the van der Waals stabilization of reactants and transition states in microporous solid catalysts. Zeolite frameworks that contain voids similar to the 8-MR pockets in MOR (DAC, AFS, AFY, SFO and EON), which are selective for the carbonylation of DME to

methyl acetate, and the 12-MR channels in MOR (NES, EON and USI), which are selective for the isopropylation of biphenyl and naphthalene to their least bulky products, are presented as potential catalytic materials.

Ray histograms and the Euclidean distances outlined here provide a tool to narrow the discovery of catalytically relevant materials with enhanced reactivity, which will ultimately depend on the connectivity of voids and the location of H^+ within them. The ray-trace code is applicable to a wide variety of porous materials and is included in the Zeo++ software for open use [18]. Histograms for zeolites from the IZA and hypothetical databases are also available publicly on the web [19].

Acknowledgements

A.J. and E.I. gratefully acknowledge the financial support from the Chevron Energy Technology Company and helpful technical discussions with Dr. Stacey I. Zones (Chevron). A.J. acknowledges with thanks a graduate research fellowship from the National Science Foundation. M.H. acknowledges support by DOE Office of Basic Energy Sciences through project #CSNEW918 entitled "Knowledge guided screening tools for identification of porous materials for CO_2 separations", and as part of the Center for Gas Separations Relevant to Clean Energy Technologies, an Energy Frontier Research Center funded by the U.S. Department of Energy, Office of Science, Office of Basic Energy Sciences under Award Number DE-SC0001015. Lawrence Berkeley National Laboratory is supported by the U.S. Department of Energy under Contract No. DE-AC02-05CH11231. The technical editing of Dr. George D. Meitzner is gratefully acknowledged.

Appendix A. Supplementary data

Supplementary data associated with this article can be found, in the online version, at http://dx.doi.org/10.1016/j.micromeso.2013.07.033.

References

[1] J. Čejka, A. Corma, S. Zones, Zeolites and Catalysis: Synthesis Reactions and Applications, John Wiley & Sons, 2010.
[2] T.F. Degnan, J. Catal. 216 (2003) 32–46.
[3] A. Corma, Chem. Rev. 95 (1995) 559–614.
[4] E.G. Derouane, P. Dejaifve, J.B. Nagy, J. Mol. Catal. 3 (1978) 453–457.
[5] E.G. Derouane, J. Catal. 100 (1986) 541–544.
[6] R.T. Carr, M. Neurock, E. Iglesia, J. Catal. 278 (2011) 78–93.
[7] R. Gounder, A.J. Jones, R.T. Carr, E. Iglesia, J. Catal. 286 (2012) 214–223.
[8] J. Čejka, G. Centi, J. Perez-Pariente, W.J. Roth, Catal. Today 179 (2012) 2–15.
[9] C.M. Baerlocher, L.B., Database of Zeolite Structures. http://www.iza-structure.org/databases.
[10] R. Pophale, P.A. Cheeseman, M.W. Deem, PCCP 13 (2011) 12407–12412.
[11] R.L. Martin, T.F. Willems, L.C. Lin, J. Kim, J.A. Swisher, B. Smit, M. Haranczyk, ChemPhysChem 13 (2012) 3595–3597.
[12] M.D. Foster, I. Rivin, M.M.J. Treacy, O.D. Friedrichs, Microporous Mesoporous Mater. 90 (2006) 32–38.
[13] E.L. First, C.E. Gounaris, J. Wei, C.A. Floudas, PCCP 13 (2011) 17339–17358.
[14] R.L. Martin, B. Smit, M. Haranczyk, J. Chem. Inf. Model. 52 (2012) 308–318.
[15] D.A. Carr, M. Lach-Hab, S.J. Yang, I.I. Vaisman, E. Blaisten-Barojas, Microporous Mesoporous Mater. 117 (2009) 339–349.
[16] N.A. Anurova, V.A. Blatov, G.D. Ilyushin, D.M. Proserpio, J. Phys. Chem. C 114 (2010) 10160–10170.
[17] M.M. Pinheiro, R.L. Martin, C.H. Rycroft, A.J. Jones, E. Iglesia, M. Haranczyk, J. Mol. Graph. Model. 44 (2013) 208–219.
[18] T.F. Willems, C.H. Rycroft, M. Kazi, J.C. Meza, M. Haranczyk, Microporous Mesoporous Mater. 149 (2012) 134–141.
[19] M. Haranczyk, Zeo++. http://www.carboncapturematerials.org/Zeo++.
[20] M. Haranczyk, J.A. Sethian, J. Chem. Theory Comput. 6 (2010) 3472–3480.
[21] E. Haldoupis, S. Nair, D.S. Sholl, J. Am. Chem. Soc. 132 (2010) 7528–7539.
[22] M.M.J. Treacy, M.D. Foster, Microporous Mesoporous Mater. 118 (2009) 106–114.
[23] L. Grajciar, J. Cejka, A. Zukal, C.O. Arean, G.T. Palomino, P. Nachtigall, ChemSusChem 5 (2012) 2011–2022.
[24] H.V. Bekkum, Introduction to Zeolite Science and Practice, Elsevier, 2001.
[25] E.G. Derouane, Microporous Mesoporous Mater. 104 (2007) 46–51.
[26] R. Gounder, E. Iglesia, Acc. Chem. Res. 45 (2012) 229–238.
[27] M. Schenk, B. Smit, T.J.H. Vlugt, T.L.M. Maesen, Angew. Chem. Int. Ed. 40 (2001) 736–739.
[28] B. Smit, T.L.M. Maesen, Nature 451 (2008) 671–678.
[29] W.O. Haag, R.M. Lago, P.B. Weisz, Faraday Discuss. 72 (1981) 317–330.
[30] A. Bhan, A.D. Allian, G.J. Sunley, D.J. Law, E. Iglesia, J. Am. Chem. Soc. 129 (2007) 4919–4924.
[31] M. Boronat, C. Martinez-Sanchez, D. Law, A. Corma, J. Am. Chem. Soc. 130 (2008) 16316–16323.
[32] Y. Sugi, H. Maekawa, Y. Hasegawa, H. Naiki, K. Komura, Y. Kubota, Catal. Today 132 (2008) 27–37.
[33] Y. Sugi, S. Tawada, T. Sugimura, Y. Kubota, T. Hanaoka, T. Matsuzaki, K. Nakajima, K. Kunimori, Appl. Catal., A 189 (1999) 251–261.
[34] Y. Sugi, M. Toba, Catal. Today 19 (1994) 187–212.
[35] R.J. Davis, Heterogen. Chem. Rev. 1 (1994) 41–53.
[36] J.T. Miller, N.G.B. Agrawal, G.S. Lane, F.S. Modica, J. Catal. 163 (1996) 106–116.
[37] J.R. Bernard, J. Nury, US Patent 4,104,320 (1976).
[38] T.M. Wortel, US Patent 4,677,236 (1986).
[39] T.R. Hughes, W.C. Buss, US Patent 4,435,283 (1984)
[40] E. Iglesia, J.E. Baumgartner, in: L. Guczi, F. Solymosi, P. Tetenyi (Eds.), Stud. Surf. Sci. Catal., vol. 75, Elsevier, Amsterdam, 1993, pp. 993–1006.
[41] R.E. Jentoft, M. Tsapatsis, M.E. Davis, B.C. Gates, J. Catal. 179 (1998) 565–580.
[42] P. Meriaudeau, C. Naccache, Catal. Rev. Sci. Eng. 39 (1997) 5–48.